Progress In Electromagnetics Research C, Vol. 67, 49–57, 2016

An Improved DBF Processor with a Large Receiving Antenna for Echoes Separation in Spaceborne SAR

Hongbo Mo[1, *], Wei Xu[2], and Zhimin Zeng[1]

Abstract—Digital beamforming (DBF) on receive in elevation with a large receiving antenna will be widely adopted in future spaceborne synthetic aperture radar (SAR) missions to improve system performances. Furthermore, DBF can be used to separate echoes corresponding to different sub-pulses in some novel spaceborne SAR imaging modes. This paper proposes an improved DBF processor with a large receiving antenna for separating echoes. The proposed DBF processor includes three important parts: multiples sharp receiving beam generation, range compression and null steering. Compared with the conventional DBF processor in spaceborne SAR, the proposed DBF processor can separate echoes with better performances. Simulation results on point targets demonstrate validity of the proposed DBF processor.

1. INTRODUCTION

Future spaceborne microwave remote sensing missions require synthetic aperture radar (SAR) systems to obtain high resolution wide swath imaging (HRWS) capacity [1–3]. The limitation between azimuth resolution and range swath is well resolved by introducing azimuth multichannel on receive technique. In addition to overcome the limitation, improving signal to noise ratio (SNR) and suppression range ambiguity should also be considered during SAR system design. Digital beamforming (DBF) on receive with a large receiving antenna in elevation in spaceborne SAR can form a sharp high gain scanning beam to receive radar echoes, and this method is named as the SCORE (SCan-On-REceive) technique [4–7]. Afterwards, the desired radar echoes arrive at the receiving antenna with a high antenna gain, while range ambiguities arrive at the receiving antenna with a low antenna gain. Therefore, the DBF on receive method in elevation can be adopted to obviously improve system performances, especially for range ambiguity to signal ratio (RASR) and noise equivalent sigma zero (NESZ).

To further improve the HRWS imaging capacity, multiple innovative spaceborne SAR imaging modes with the scheme of several sub-pulses transmitted with different time delays in a single pulse repetition interval (PRI) have been proposed in recent years [7–12]. The key point of processing SAR data of these modes is echoes separation corresponding to different sub-pulses [7, 12–14]. As different sub-pulses are transmitted with different time delays, their corresponding echoes in the mixed receiving window can be separated by a DBF processor to form a sharp receiving beam in elevation based on the time delay and the side looking SAR imaging geometry.

This paper proposes an improved DBF processor with null steering to separate echoes corresponding to different sub-pulses. The proposed improved processor includes three important steps. First, the large receiving antenna in elevation forms several sharp receiving beams to scan on receiving echoes corresponding to different sub-pulses according to the side looking SAR imaging geometry. Afterwards, echoes received by different antenna beams are individually compressed. The final step for null steering

Received 26 May 2016, Accepted 16 August 2016, Scheduled 8 September 2016

* Corresponding author: Hongbo Mo (mohongbo@bupt.edu.cn).

[1] School of Information and Communication Engineering and Beijing Key Laboratory of Network System Architecture and Convergence, Beijing University of Posts and Telecommunications, Beijing 100876, China. [2] Spaceborne Microwave Remote Sensing System Department, Institute of Electronics, Chinese Academy of Sciences, Beijing 100190, China.

is operated to further improve the effect of echoes separation for different sub-pulses. To validate the proposed processor, simulation experiments on point targets are carried out.

This paper is organized as follows. Section 2 reviews the innovative imaging scheme with multiple sub-pulses transmitted in a single PRI and real time DBF on receive in spaceborne SAR. Section 3 is focused on presenting the proposed improved DBF processor for echoes separation. Simulation results on point targets are given in Section 4 to validate the proposed approach. Finally, this paper is concluded in Section 5.

2. DBF ON RECEIVE IN ELEVATION

In conventional spaceborne SAR systems, only a pulse is transmitted in a single PRI. However, multiple innovative SAR imaging modes with several transmitted sub-pulses in a single PRI as shown in Fig. 1(a) are proposed to improve the HRWS capacity in recent years. These sub-pulses are with the same carrier frequency and phase coding but different transmitted time delays. Echoes corresponding to different sub-pulses are mixed in the receiving window as shown in Fig. 1(b). Fortunately, the mixed echoes corresponding to sub-pulse 1 and sub-pulse 2 arrive at the receiving antenna with different directions such as point targets P and Q in Fig. 1. As a result, echoes corresponding to different sub-pulses can be separated by the sharp receiving beam according to the relationship between the time delay and the side looking SAR imaging geometry.

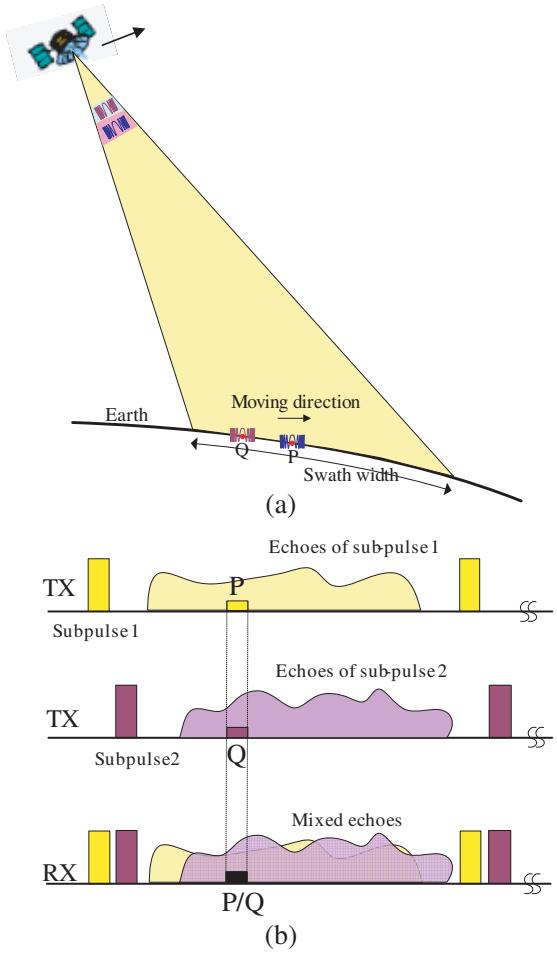

Figure 1. Spaceborne SAR imaging scheme with two sub-pulses transmitted in a single PRI. (a) The spaceborne imaging geometry. (b) The receiving window.

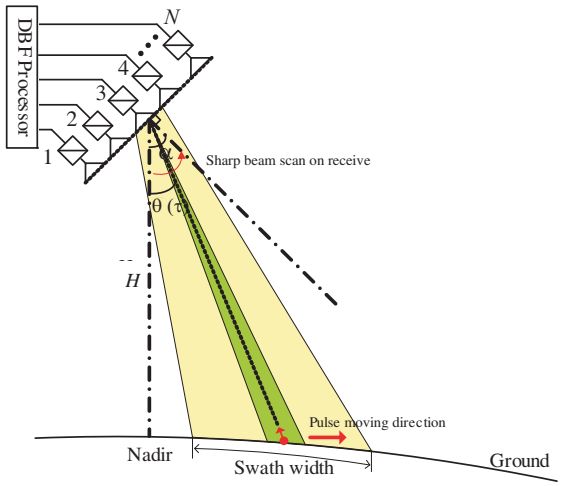

Figure 2. The spaceborne imaging geometry of DBF on receive in elevation.

Figure 2 shows the imaging geometry of DBF on receive in elevation, where the large receiving antenna is divided into N sub-apertures, and each sub-aperture receives and records radar echoes individually. The normal direction of the receiving array antenna in elevation is denoted as α, and the radar echo arriving direction $\theta(\tau)$ can be easily obtained according to the spaceborne SAR imaging geometry as follows:

$$\theta(\tau) = \arccos \sqrt{\frac{(R_e + H)^2 + (c\tau/2)^2 - R_e^2}{2(R_e + H) \cdot c\tau}} \tag{1}$$

where τ is the fast time, R_e the Earth radius, H the satellite height, and c the light speed.

The demodulated baseband radar echo of the n-th sub-aperture can be expressed as:

$$s_n(\tau) = \text{rect}\left[\frac{\tau - \tau_n}{\tau_p}\right] \cdot \exp\left[j2\pi f_c(\tau - \tau_n) + j\pi K_r(\tau - \tau_n)^2\right] \tag{2}$$

with

$$\tau_n = \tau_d - \frac{(n-1) \cdot d \cdot \sin(\theta_0 - \alpha)}{c} = \tau_d - \Delta\tau_n \tag{3}$$

where τ_p indicates the pulse duration, τ_d the time delay between the radar pulse transmit and its corresponding echo receiving at the first sub-aperture as shown in Fig. 2, f_c the carrier frequency, K_r the transmitted pulse chirp rate, and θ_0 the actual direction of arrival (DOA) of the received echoes. According to the working principle of an array antenna, the multiplied beam steering vector $\mathbf{w}(\tau)$ to form a sharp beam to receive echoes with the direction of $\theta(\tau)$ is as follows:

$$\mathbf{w}(\tau) = [w_1, w_2, \ldots, w_N] \tag{4}$$

with

$$w_n(\tau) = \exp\left\{-j2\pi \frac{(n-1) \cdot d}{\lambda} \cdot \sin[\theta(\tau) - \alpha]\right\} \tag{5}$$

Using the principle of stationary phase (POSP), the spectrum of the received signal in the n-th channel after multiplying the steering vector $\mathbf{w}(\tau)$ can be easily obtained and expressed as follows [14]:

$$\begin{aligned} S_n(f) \;=\; & C \cdot \exp\{-j2\pi(f + f_c)\tau_d\} \cdot \text{rect}\left[\frac{f + (n-1) \cdot f_0}{K_r \tau_p}\right] \cdot \exp\left\{-j\frac{\pi}{K_r} f^2\right\} \\ & \cdot \exp\left\{j2\pi f\left(\Delta\tau_n - \frac{(n-1)}{K_r} \cdot f_0\right)\right\} \end{aligned} \tag{6}$$

with

$$f_0 = \frac{d}{\lambda} \cdot \cos[\theta(\tau_c) - \alpha] \cdot \frac{\partial\theta(\tau_c)}{\partial\tau} \tag{7}$$

According to the spectrum in Eq. (6), the linear phase term should be compensated as follows:

$$H_{f,n}(f) = \exp\left\{-j2\pi f\left(\Delta\tau_n - \frac{(n-1) f_0}{K_r}\right)\right\} \tag{8}$$

This step can also be implemented in the time domain via time delay D_n as follows:

$$D_n = \Delta\tau_n - \frac{(n-1) f_0}{K_r} \tag{9}$$

Therefore, a sharp high gain scanning beam to receive echoes is implemented via a multiplied vector and a set of time delayers. The block diagram of the real time conventional DBF processor in elevation onboard is shown in Fig. 3.

According to Eqs. (8) and (9), the time delayers in Fig. 3 can be implemented by two methods as shown in Fig. 3. For the first method operated in the frequency domain as shown in Fig. 4(a), the whole raw data of each pulse in each elevation channel should be pre-stored in a buffer at first and then transformed into the frequency domain to compensate the linear phase term via multiplying the phase function in Eq. (8). Consequently, the raw data from all elevation channels are combined in the frequency domain, and then the resulting data are transformed into the time domain before block

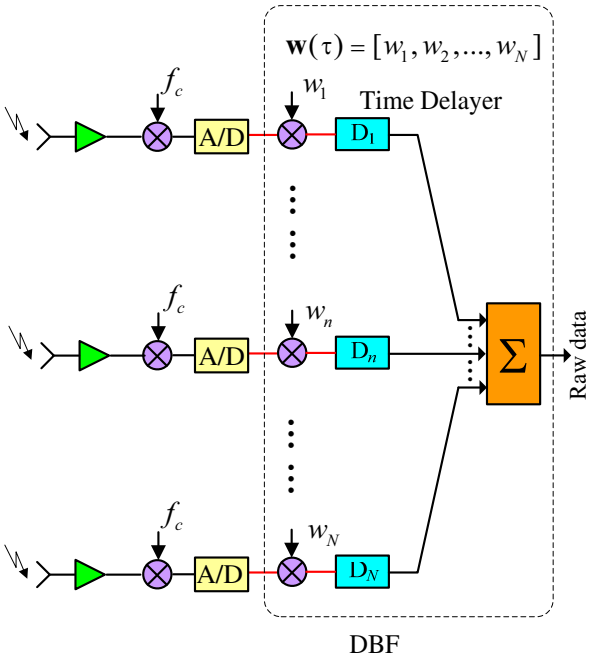

Figure 3. The block diagram of the real time conventional DBF processor in elevation onboard.

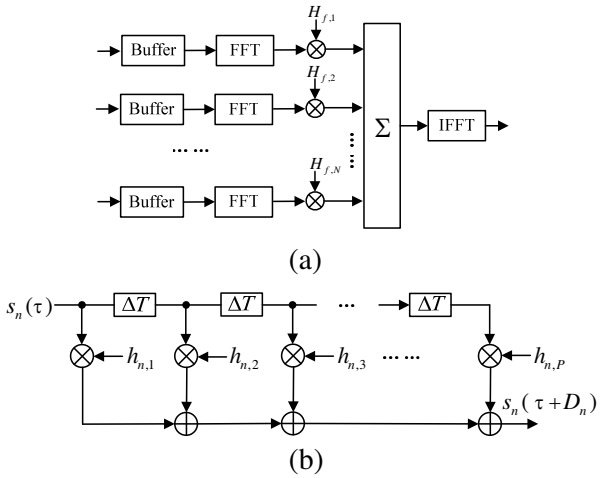

Figure 4. Implementation of the time delay in Fig. 3. (a) Implemented by the phase compensation in the frequency domain. (b) Implemented by the finite impulse response (FIR) filter.

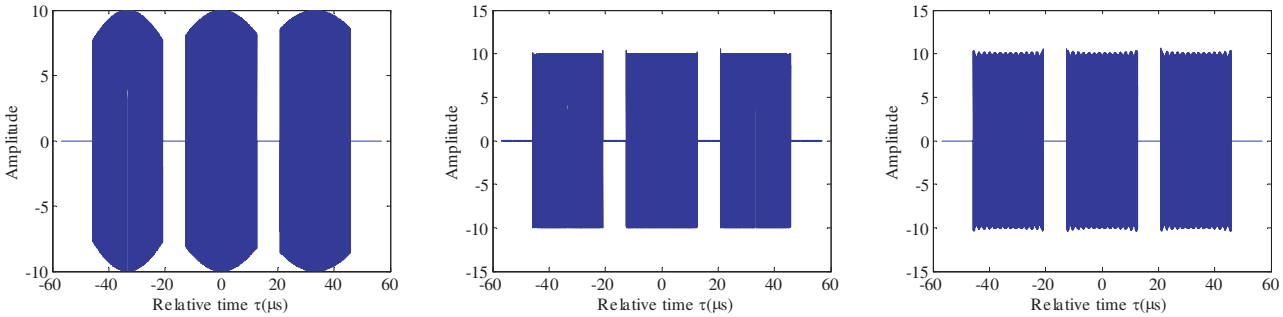

Figure 5. Simulation results of DBF on receive in elevation. (a) Without any time delays. (b) The time delay implemented in the Doppler domain. (c) The time delay implemented by the sinc interpolator.

adaptive quantization (BAQ) data compression onboard. As we know, the time delay in digital signal processing can be implemented via N-order finite impulse response (FIR) filter as shown in Fig. 4(b), where $h_{n,p}$ $(p = 1, 2, 3, \ldots, P)$ indicates the interpolation kernel function of the N-order FIR filter.

Figure 5 shows simulation results of DBF in elevation with different methods, and simulation parameters are listed in Table 1. Just multiplying the steering vector $\mathbf{w}(\tau)$, the amplitude of radar echoes will be obviously reduced as shown in Fig. 5(a) due to different spectrum shifts in different elevation channels in Eq. (6), while the raw data from all elevation channels are well combined via methods in Figs. 4(b) and (c). The little fluctuation of amplitude of the combined signal as shown in Fig. 5(c) is mainly caused by limited order of the FIR filter, and the FIR filter is 16-order in Fig. 5(c).

3. IMPROVED DBF PROCESSOR FOR ECHO SEPARATION

A block diagram of the proposed improved DBF processor for echoes separation is shown in Fig. 6, and the proposed processor includes three steps: multiple sharp scanning beams generation, range compression and interference echoes suppression by null steering. In Fig. 6, the number of sub-apertures in elevation and the number of sub-pulses transmitted in a single PRI are assumed as N and K, respectively, and N is larger than K.

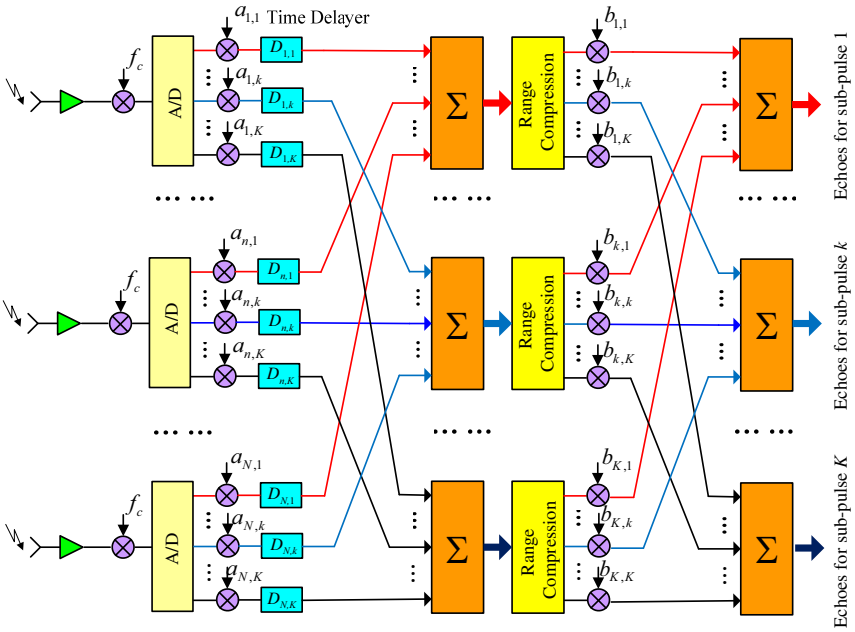

Figure 6. Block diagram of the proposed improved DBF processor for echoes separation.

The first step of the proposed DBF processor for multiple sharp scanning beams generation is controlled by the steering matrix $\mathbf{A}(\tau)$ and a series of time delayers as show in Fig. 6. The steering matrix $\mathbf{A}(\tau)$ can be expressed as follows:

$$\mathbf{A}(\tau) = \begin{bmatrix} \mathbf{a}_1(\tau) \\ \mathbf{a}_2(\tau) \\ \vdots \\ \mathbf{a}_K(\tau) \end{bmatrix} = \begin{bmatrix} a_{1,2} & a_{1,2} & \cdots & a_{1,N} \\ a_{2,2} & a_{2,2} & \cdots & a_{2,N} \\ \vdots & \vdots & \ddots & \vdots \\ a_{K,1} & a_{K,2} & \cdots & a_{K,N} \end{bmatrix} \tag{10}$$

with

$$\mathbf{a}_k(\tau) = \left[1, \exp\left(-j\frac{2\pi}{\lambda}d \cdot \sin\theta_k(\tau)\right), \ldots, \exp\left(-j\frac{2\pi}{\lambda}(N-1) \cdot d \cdot \sin\theta_k(\tau)\right)\right]^T \tag{11}$$

where symbol $(\cdot)^T$ denotes the transpose operator, and $\theta_k(\tau)$ indicates the sharp receiving beam pointing direction for the k-th sub-pulse. The time delayer $D_{n,k}$ is described as follows:

$$D_{n,k} = \Delta\tau_{n,k} - \frac{(n-1)\,f_0}{K_r} = \frac{(n-1) \cdot d \cdot \sin(\theta_{0,k} - \alpha)}{c} - \frac{(n-1)\,f_0}{K_r} \tag{12}$$

where $\theta_{0,k}$ indicates the DOA of the received echoes for the k-th sub-pulse.

The energy of radar echoes is scattered throughout the whole pulse duration before range compression, and it is very hard to separate echoes corresponding to different sub-pulses from different range bins. Therefore, range compression of the raw data received by each sharp beam should be taken before the null steering step. After range compression, echo received by the k-th scanning sharp

receiving beam is expressed as

$$s_k(\tau) = \mathbf{a}_k^T(\tau)\left[\mathbf{u_1}(\tau), \mathbf{u_2}(\tau), \ldots, \mathbf{u}_K(\tau)\right] \begin{bmatrix} \sigma_1(\tau) \\ \sigma_2(\tau) \\ \cdots \\ \sigma_K(\tau) \end{bmatrix} \tag{13}$$

with

$$\mathbf{u}_k(\tau) = \left[1, \exp\left(j\frac{2\pi}{\lambda}d \cdot \sin\theta_k(\tau + D_{2,k})\right), \ldots, \exp\left(j\frac{2\pi}{\lambda}(N-1) \cdot d \cdot \sin\theta_k(\tau + D_{N,k})\right)\right]^T \tag{14}$$

where $\sigma_k(\tau)$ indicates the range compressed radar echoes for the k-th sub-pulse. As a result, echoes received by all sharp receiving beam can be written as

$$s_k(\tau) = \begin{bmatrix} \mathbf{w}_1(\tau) \\ \mathbf{w}_2(\tau) \\ \cdots \\ \mathbf{w}_k(\tau) \end{bmatrix} \left[\mathbf{u_1}(\tau), \mathbf{u_2}(\tau), \ldots, \mathbf{u}_K(\tau)\right] \begin{bmatrix} \sigma_1(\tau) \\ \sigma_2(\tau) \\ \cdots \\ \sigma_K(\tau) \end{bmatrix} = \mathbf{C}(\tau) \begin{bmatrix} \sigma_1(\tau) \\ \sigma_2(\tau) \\ \cdots \\ \sigma_K(\tau) \end{bmatrix} \tag{15}$$

with

$$\mathbf{w}_k(\tau) = \left[1, \exp\left(-j\frac{2\pi}{\lambda}d \cdot \sin\theta_k(\tau + D_{2,k})\right), \ldots, \exp\left(-j\frac{2\pi}{\lambda}(N-1) \cdot d \cdot \sin\theta_k(\tau + D_{N,k})\right)\right]^T \tag{16}$$

According to Eq. (15), the matrix $\mathbf{B}(\tau)$ in Fig. 6 for null steering is easily obtained as follows:

$$\mathbf{B}(\tau) = \begin{bmatrix} b_{1,1} & \ldots & b_{1,K} \\ \vdots & \ddots & \vdots \\ b_{K,1} & \ldots & b_{K,K} \end{bmatrix} = \mathbf{C}^{-1}(\tau) = \begin{bmatrix} c_{1,1} & \ldots & c_{1,K} \\ \vdots & \ddots & \vdots \\ c_{K,1} & \ldots & c_{K,K} \end{bmatrix}^{-1} \tag{17}$$

with

$$c_{p,q}(\tau) = \sum_n^N \exp\left\{j\frac{2\pi}{\lambda}d \cdot (n-1) \cdot \left[\sin\left(\theta_q(\tau_n + D_{n,q})\right) - \sin\left(\theta_p(\tau_n + D_{n,p})\right)\right]\right\}, \text{ with } p, q = 1, 2, \ldots, K \tag{18}$$

Compared with the conventional DBF on receive method, the proposed DBF processor introduces null steering operation to improve performances of echoes separation corresponding to different sub-pulses. Furthermore, range compression for each receiving beam is carried out before the final null steering operation. The first step for multiple sharp scanning beams generation is implemented onboard, while the following steps for range compression and null steering can be finished on the ground. As the last two steps of the proposed DBF processor are operated on the ground, it will not increase any computation burden onboard compared with the conventional DBF on receive method. Furthermore, the data rate of the proposed DBF processor is the same as that of the conventional DBF processor.

4. SIMULATION EXPERIMENT

To validate the proposed DBF processor for echo separation, simulation experiments on point targets are carried out. Simulation parameters are listed in Table 1.

Assuming that there a point target in the imaged swath center, Fig. 7 shows simulation results of the conventional DBF processor, the DBF processor in [14] and the proposed DBF in this paper. Compared with results of the conventional DBF processor and the DBF processor in [14], undesired echoes are better suppressed in the proposed approach, which means that the proposed DBF processor with null steering shows better performance for echoes separation.

To further validate the proposed DBF processor for echoes separation, a simulation experiment on four point targets with different range locations is carried out. Simulation results are shown in Fig. 8 and also validate a better performance of the proposed DBF processor for echoes separation. Furthermore, a new term isolation level (IL) is introduced to describe the rate of the desired echo and interference echo, and IL of four point targets handled by different DBF processors in Fig. 8 are summarized and listed in Table 2. Compared with the DBF processor in [14], the IL is lifted by more than 10 dB.

Table 1. Simulation parameters for echoes separation.

Simulation parameters	value
Sensor height	675 km
Side looking angle	25°
Pulse duration	40 μs
Pulse bandwidth	150 MHz
Sampling frequency	180 MHz
The height of the receiving antenna	2.56 m
The height of the sub-aperture	0.32 m
Number of sub-apertures	8
Number of sub-pulses in a PRI	2
The time delay between two sub-pulses	45 μs

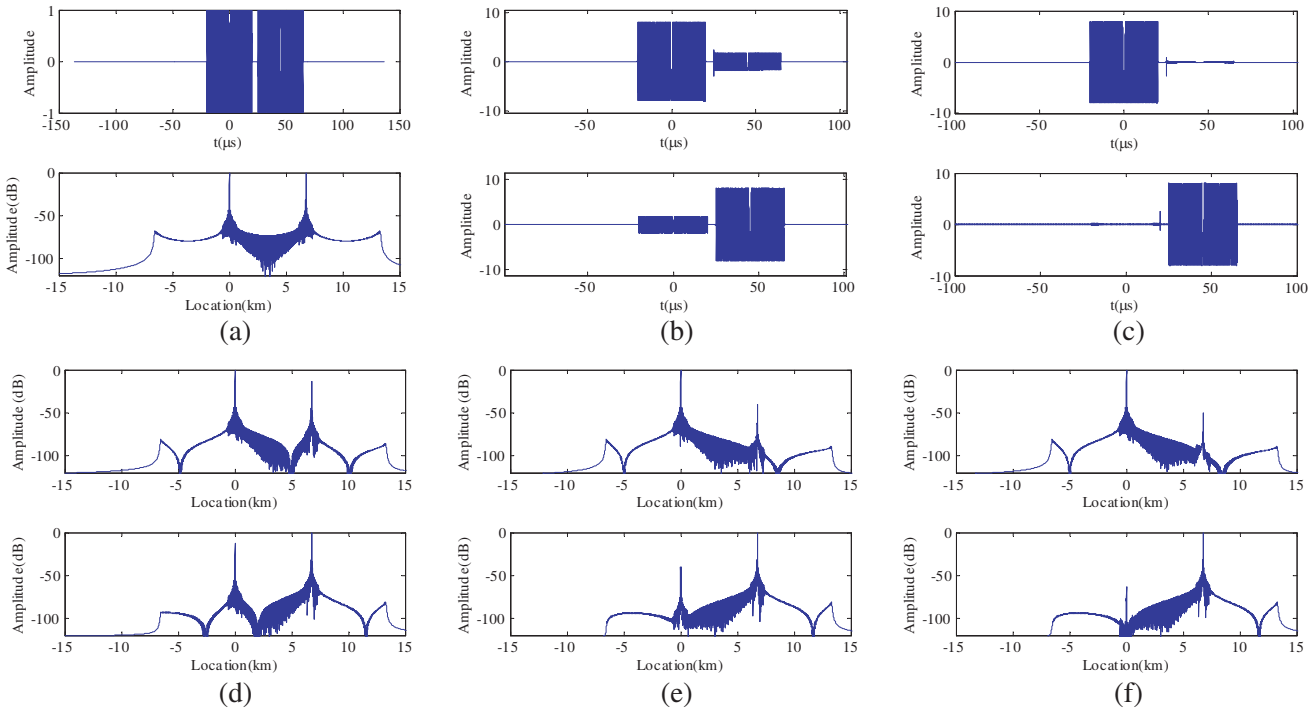

Figure 7. Simulation results of a single point target. (a) The real part of received echo in an individual elevation channel (top), the compressed data (bottom). (b) Echo separation results of the conventional DBF processor for the posterior beam (top) and the anterior beam (bottom). (c) Echo separation results of the null steering DBF processor in [14] for the posterior beam (top) and the anterior beam (bottom). (d) Compressed echo separation results of the conventional DBF processor for the posterior beam (top) and the anterior beam (bottom). (e) Compressed echo separation results of the null steering DBF processor in [14] for the posterior beam (top) and the anterior beam (bottom). (e) Compressed echo separation results of the proposed DBF processor for the posterior beam (top) and the anterior beam (bottom).

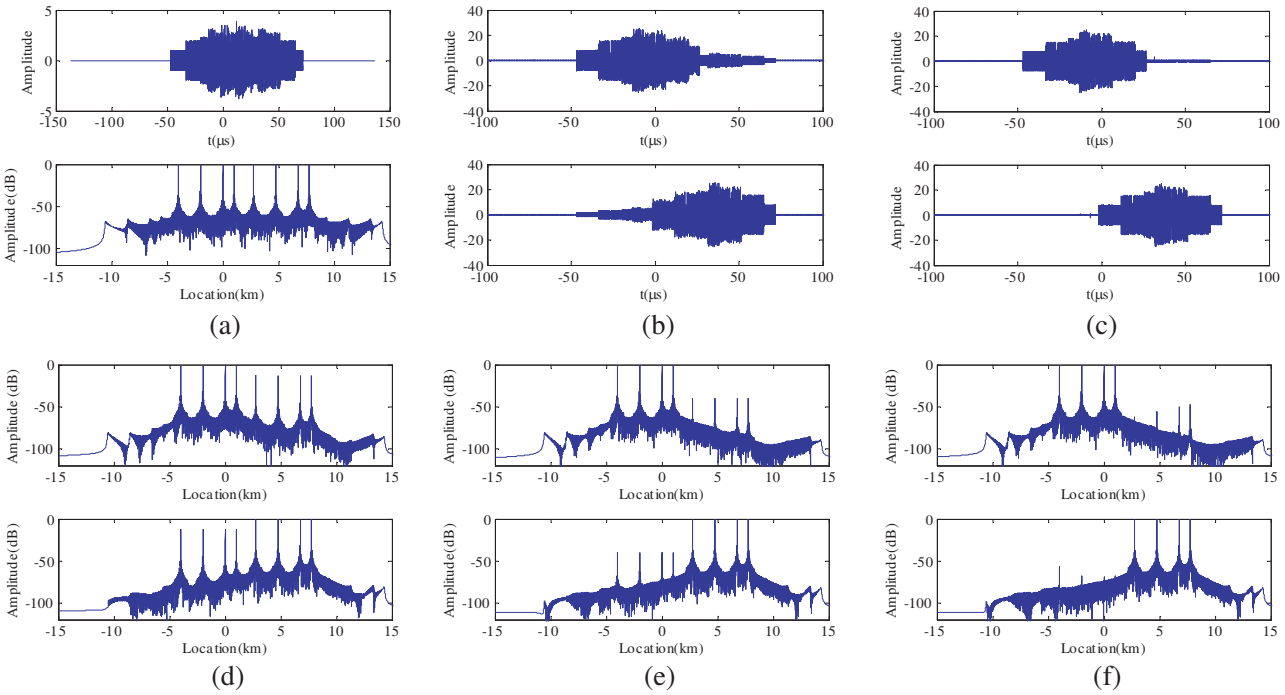

Figure 8. Simulation results of multiple point targets. (a) The real part of received echo in an individual elevation channel (top), the compressed data (bottom). (b) Echo separation results of the conventional DBF processor for the posterior beam (top) and the anterior beam (bottom). (c) Echo separation results of the null steering DBF processor in [14] for the posterior beam (top) and the anterior beam (bottom). (d) Compressed echo separation results of the conventional DBF processor for the posterior beam (top) and the anterior beam (bottom). (e) Compressed echo separation results of the null steering DBF processor in [14] for the posterior beam (top) and the anterior beam (bottom). (e) Compressed echo separation results of the proposed DBF processor for the posterior beam (top) and the anterior beam (bottom).

Table 2. Echoes separation result comparison of different DBF processors.

IL / Approach	IL for receiving beam 1 (dB)				IL for receiving beam 2 (dB)			
	P1	P2	P3	P4	P1	P2	P3	P4
Conventional DBF processor	12.89	13.01	13.18	13.29	12.90	12.82	12.80	12.80
DBF processor in [14]	39.82	40.19	40.38	40.51	39.98	39.87	39.89	39.89
Proposed processor	62.35	55.72	51.02	49.93	56.57	67.90	68.48	68.04

5. CONCLUSION

The image schemes with multiple sub-pulses transmitted in a single PRI can improve the HRWS capacity of the spaceborne SAR system and have been hotly discussed in recent years. The key point of data processing of these schemes is echoes separation corresponding to different sub-pulses. This paper proposes an improved DBF processor for echoes separation, which includes three processing steps: multiple sharp scanning beams generation, range compression and null steering. Compared with simulation results of DBF processors for echoes separation, the proposed approach shows better

performance. As the last steps of the proposed DBF processor can be implemented on the ground, the proposed processor does not increase any computation burden and data rate onboard

ACKNOWLEDGMENT

This work is supported by the NSF of China (No. 61271177).

REFERENCES

1. Gebert, N., "Multi-channel azimuth processing for high-resolution wide-swath SAR imaging," Ph.D. dissertation, Univ. Karlsruhe, Karlsruhe, Germany, 2009.
2. Currie, A. and M. A. Brown, "Wide-swath SAR," *Proc. Inst. Electr. Eng. F — Radar Signal Process.*, Vol. 139, No. 2, 122–135, Apr. 1992.
3. Callaghan, G. D. and I. D. Longstaff, "Wide-swath space-borne SAR using a quad-element array," *Proc. Inst. Electr. Eng. — Radar, Sonar Navig.*, Vol. 146, No. 3, 159–165, Jun. 1999.
4. Suess, M., B. Grafmueller, and R. Zahn, "A novel high resolution, wide swath SAR system," *Proc. IEEE Int. Geosci. Remote Sens. Symp.*, 1013–1015, Sydney, Australia, 2001.
5. Suess, M. and W. Wiesbeck, "Side-looking synthetic aperture radar system," Euro Patent EP 1 241 487 A1, 2001.
6. Krieger, G., N. Gebert, M. Younis, and A. Moreira, "Advanced synthetic aperture radar based on digital beamforming and waveform diversity," *Proc. IEEE Radar Conf.*, 1–6, 2008.
7. Krieger, G., N. Gebert, and A. Moreira, "Multidimensional waveform encoding: A new digital beamforming technique for synthetic aperture radar remote sensing," *IEEE Trans. Geosci. Remote Sens.*, Vol. 46, No. 1, 31–46, Jan. 2008.
8. Wang, W.-Q., "Space-time coding MIMO-OFDM SAR for high-resolution imaging," *IEEE Trans. Geosci. Remote Sens.*, Vol. 49, No. 8, 3094–3104, Aug. 2011.
9. Wang, W.-Q., "Virtual antenna array analysis for MIMO synthetic aperture radars," *Int. J. Antennas Propag.*, Vol. 2012, 276, 587, 2012.
10. Wang, W.-Q., "Mitigating range ambiguities in high-PRF SAR with OFDM waveform diversity," *IEEE Geosci. Remote Sens. Lett.*, Vol. 10, No. 1, 101–105, Jan. 2013.
11. Krieger, G., "MIMO-SAR: Opportunities and pitfalls," *IEEE Trans. Geosci. Remote Sens.*, Vol. 52, No. 5, 2628–2645, May 2014.
12. Kim, J., M. Younis, A. Moreira, and W. Wiesbeck, "A novel OFDM chirp waveform scheme for use of multiple transmitters in SAR," *IEEE Geosci. Remote Sens. Lett.*, Vol. 10, No. 3, 568–572, May 2013.
13. Xu, W., Y. Deng, and R. Wang, "Multichannel synthetic aperture radar systems with a planar antenna for future spaceborne microwave remote sensing," *IEEE Aerospace and Electronic Systems Magazine*, Vol. 46, No. 12, 26–30, Dec. 2012.
14. Feng, F., S. Li, W. Yu, P. Huang, and W. Xu, "Echo separation in multi-dimensional waveform encoding SAR remote sensing using an advanced null-steering beamformer," *IEEE Trans. Geosci. Remote Sens.*, Vol. 50, No. 10, 4157–4172, Oct. 2012.